A Combined Spectroscopic and Computational Investigation on the Solvent-to-Chromophore Excited-State Proton Transfer in the 2,2'-Pyridylbenzimidazole-Methanol Complex

Ramesh Jarupula,[‡,a] Saurabh Khodia,[‡,a] Md. Shabeeb,[a] and Surajit Maity*[a]

Abstract: This article demonstrated experimental proof of excited state 'solvent-to-chromophore' proton transfer (ESPT) in the isolated gas phase PBI (2,2'-pyridylbenzimidazole)-CH_3OH complex, aided by computational calculation. The binary complexes of PBI with CH_3OH/CH_3OD were produced in a supersonic jet-cooled molecular beam and the energy barrier of the photo-excited process was determined using resonant two-colour two-photon ionization spectroscopy (R2PI). The ESPT process in the PBI-CH_3OH complex was confirmed by the disappearance of the Franck-Condon active vibrational transitions above 0_0^0+390 cm^{-1}. In the PBI-CH_3OD complex, the reappearance of the Franck-Condon till 0_0^0+800 cm^{-1} confirmed the elevation of the ESPT barrier upon isotopic substitution due to the lowering of the zero-point vibrational energy. The ESPT energy barrier in PBI-CH_3OH was bracketed as 410±20 cm^{-1} (4.91±0.23 kJ mol^{-1}) by comparing the spectra of PBI-CH_3OH and PBI-CH_3OD. The solvent-to-chromophore proton transfer was confirmed based on the significantly decreased quantum tunnelling of the solvent proton in the PBI-CH_3OD complex. The computational investigation resulted in an energy barrier of 6.0 kJ mol^{-1} for the ESPT reaction in the PBI-CH_3OH complex, showing excellent agreement with the experimental value. Overall, the excited state reaction progressed through an intersection of ππ* and nπ* states before being deactivated to the ground state via internal conversion. The present investigation reveals a novel reaction pathway on the deactivation mechanism of the photo-excited N-containing biomolecules in the presence of protic-solvents.

Keywords: ESPT process, Laser spectroscopy, Gas phase complexes, Hydrogen bonding, Energy barrier

Introduction:

The deactivation of photo-excited molecules is the key mechanism by which nature protects important biological entities from UV-induced destruction.[1–4] Over the last couple of decades, the advancement of highly accurate experimental and theoretical techniques has helped us better understand deactivation processes. The solvent-assisted proton transfer pathway has been identified as the primary deactivation route in investigations of nucleobase analogues in the condensed phase, supported by femtosecond and picosecond photophysical experiments.[5–8] The excited state proton transfer in the gas phase, from the excited chromophore to the solvent molecule, was proposed in Naphthol-$(NH_3)_n$ complexes by Knochenmuss et al..[9,10] Subsequent studies by several groups confirmed that the above processes require at least 3-4 solvent molecules to trigger the ESPT processes.[10–13] On the other hand, the gas phase studies of Phenol-$(NH_3)_n$ systems by Jouvet et al. have identified the presence of a major excited-state hydrogen transfer pathway by detecting the NH_4 radical in the gas phase, even in the 1:1 binary complex.[14] The most studied system in the gas phase clusters has been the solvent clusters of 7-azaindole derivatives. The gas phase investigations of 7AI-S_n mainly observed the deactivation and tautomerization of the complexes via the chromophore-to-solvent proton transfer mechanism.[13,15–18] In the above systems, the spectroscopic investigations, aided by the computational studies, revealed that the deactivation occurs via the transfer of the acidic hydrogen atom of the excited chromophore to the nearest hydrogen-bonded solvent molecule. The further course of the reaction depends on the hydrogen or proton transfer barriers to either the deactivation channel to the ground state or the tautomeric products.

The above-reported studies have mainly demonstrated the excited state transfer of hydrogen /proton transfer from the chromophore-to-solvent molecules. Until recently, our group has demonstrated a novel proton transfer mechanism in the 2(2'-pyridyl)-benzimidazole (PBI)–H_2O complex.[19] In the above study, the excited state proton transfer took place from solvent to chromophore via the intersection of the $^1n\pi^*$ and $^1\pi\pi^*$ states along the proton transfer coordinate. This led to the deactivation of the chromophore via internal conversion. The above process was predicted based on the subsequent experiments with PBI-D_2O and PBI-NH_3 complexes.[20] The energy barriers in the PBI-S complexes were confirmed by recording the UV-UV hole-burning spectroscopy and the R2PI spectroscopy with isotope-enriched solvents. The reaction pathway in PBI–H_2O complex was further confirmed by calculating the kinetic isotopic effect in the PBI-D_2O complex. The vibrational modes along the proton transfer coordinate exhibited quantum mechanical tunnelling in the PBI-H_2O system, which was greatly reduced in PBI-D_2O and PBI-NH_3 systems. In the earlier system, the isotopic substitution can decrease the zero-point vibrational energy in the S_1 state and the resultant higher energy barrier can be the reason for the lower tunnelling of D^+ in the system. In the case of PBI-NH_3, the tunnelling is suppressed due to the increase in the energy barrier and width of the potential, i.e., the pyridyl-N···H (solvent). A similar solvent-to-chromophore excited state proton transfer was also reported for 2,7-diazaindole-$(H_2O)_{1-3}$ complexes, and the energy barriers were calculated to be nearly similar to the respective s

[a] *Department of Chemistry, IIT Hyderabad, Kandi, Sangareddy, India 502284*
‡ Equal contribution

*surajitmaity@chy.iith.ac.in

Electronic Supplementary Information (ESI) available:

The accurate description of solvent-to-chromophore proton transfer requires further experimental data. Based on the limited experimental data, it can be proposed that the ESPT process is highly dependent on the polarity of the hydrogen bond donor group of the solvent. The PBI-NH_3 did not show any evidence of ESPT up to 880 cm^{-1} above the excitation energy. In the PBI-H_2O Complex, the ESPT process was detected near 430 cm^{-1}. The above is most likely due to the higher O-H bond polarity than the N-H bond in ammonia. Methanol is marginally more acidic in the gas phase than water,[22] with similar OH bond polarity. Therefore, a similar excited state proton transfer phenomen on can be observed in the methanol complex of PBI.

In this article, we have investigated the excited state processes in PBI-CH_3OH and PBI-CH_3OD complexes. The underlying reaction mechanism was probed by measuring the (a) energy barriers in the excited state and (b) the kinetic isotope effect on the spectral bands in the PBI-CH_3OD complex. The PBI contains the basic N and acidic N-H groups that can be bridged via hydrogen bonding with a methanol molecule to facilitate proton/hydrogen transfer upon UV photoexcitation. To better understand the decay pathway of this system, computational calculations were performed in both the ground and excited states.

Method:

Experimental: The electronic spectrum of the PBI–CH_3OH complex at $S_0 \rightarrow S_1$ was measured using the resonant two-photon ionization (R2PI) technique. The PBI–methanol complex was generated using a supersonic jet expansion in a molecular beam source. A molecular beam containing methanol and PBI vapour seeded in 2 bars of He adiabatically expanded and collimated through a 3mm skimmer into a differentially pumped vacuum region. The experimental setup is provided in more detail elsewhere.[14] The PBI sample (Sigma-Aldrich, 97%) was heated to 393K in order to achieve the required vapour pressure. The temperature of the solvent holder was operated at 243K for the PBI-CH_3OH and 255K for CH_3OD using a Peltier setup to maximize the 1:1 complex. The isolated jet-cooled molecular complex was excited by the frequency-doubled output of a tunable dye laser with a bandwidth of$\sim$0.3 cm^{-1} in the visible region. The second harmonic of an Nd: YAG laser was used to pump (a) the dye laser and (b) the 4th harmonic BBO crystal to generate 266 nm for the ionization. The generated ions were recorded by monitoring the m/z ratio of 227 amu (PBI–CH_3OH) and 228 amu (PBI-CH_3OD) using one-meter linear time-of-flight (TOF) mass spectrometer equipped with an MCP detector. The UV laser beam size of $\sim$2 mm with a laser power of $\sim$ 0.2 mJ per pulse was used for all experiments.

Computational: TURBOMOLE program was used to carry out all calculations with the resolution-of-identity (RI) approximation.[23] Potential-energy profiles and the geometry optimizations in the ground and excited state were calculated at the dispersion corrected density functional theory B3LYP-D4 using the def2-TZVPP basis sets. Tamm–Dancoff approximation (TDA) was used for all the Time-Dependent Density Functional Theory (TD-DFT) calculations. The PBI–CH_3OH Complex was optimized by keeping the methanol molecule in all orientations around the PBI molecule to make a molecular bridge between the N-H group of imidazolyl (N_I-H) and the N group of pyridyl (N_P) rings. The frequency calculations at S_0 and S_1 states were done to confirm further the optimized structures at the same level of theory. The proton transfer state was optimized with the protonated PBI cation ($PBIH^+$) and a methoxide ion (CH_3O^-) to form a hydrogen bonded bridging structure.

The bond length between the N_I-H and pyridine $N_P\cdots$H were constrained for the $PBIH^+$ geometry to obtain the ground state structure of the PT state. The excited state structure of the PT was obtained without any constraints. Subsequently, the potential energy surface (PES) were calculated by scanning the N(5)-H(4) (i.e., $N_P\cdots$H) and N(1)-H(2) (i.e., N_I-H) distances in the S_0 and S_1 states and the details are explained in the respective sections. The optimization criteria were used for changes in the gradient at $10^{-4}E_h/a_0$ and convergence criteria at 10^{-6} Hartree/Bohr. The Cartesian coordinates are provided in the supporting information file for the optimized geometries of the complexes.

The FC-LabWin program developed by Pugliesi *et al.*[24] was used to calculate the Franck–Condon simulated spectrum by using the ground and the excited-state optimized geometries of the PBI-CH_3OH complex. The resolution was set at 0.5 cm^{-1} for the simulated spectrum to compare with the bandwidth of the experimentally observed spectra.

Results and discussion:

Two-colour R2PI Spectroscopy: The R2PI spectrum of the PBI–CH_3OH (Figure 1b) complex, was recorded by monitoring m/z ratios of 227 amu. The $S_0 \rightarrow S_1$ electronic band origin transitions (0_0^0) of the complex was observed at 30400 cm^{-1}, which is redshifted by 1211 cm^{-1} with respect to that of the bare PBI molecule (Figure 1a at 31611 cm^{-1}). The positions of the bands with possible assignments are given in Table 1. Both the band origin position and the spectral shift in the PBI-CH_3OH complex are nearly identical to that reported earlier.[25]

The position of the 0_0^0 band was proved to be a vital role in determining the docking site of the solvent on PBI molecule.[19,26] The 0_0^0 band of the PBI-Ar, PBI-H_2O complexes were reported to display a redshift of 40 cm^{-1}, and 1067 cm^{-1}.[19,26,27] Note that, the band origin of the π-bound PBI-Ar cluster displayed a marginal shift, whereas the OH$\cdots$N and NH$\cdots$O hydrogen bonded PBI-H_2O have

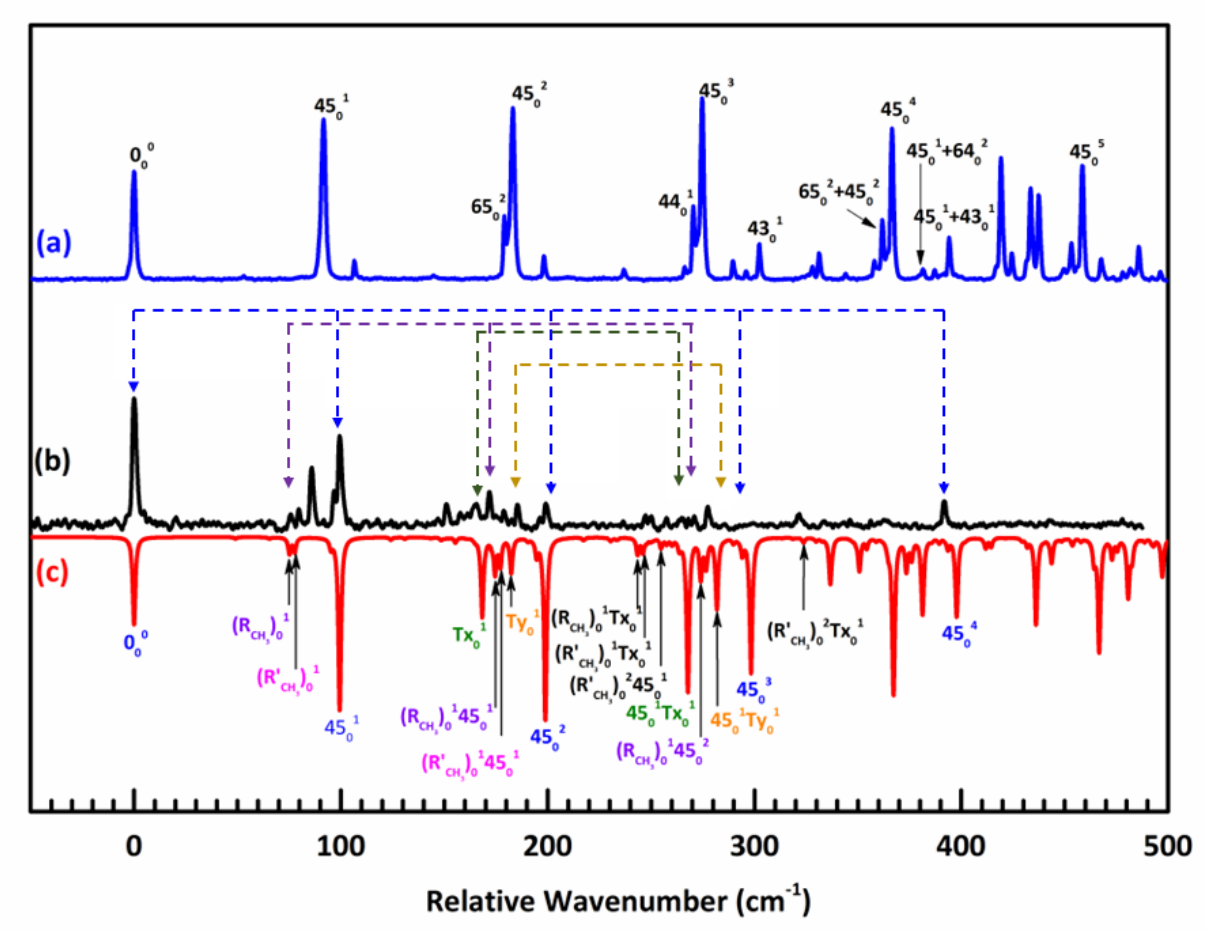

Figure 1. Two-colour resonant two-photon ionization spectra of the $S_0 \rightarrow S_1$ transitions in (a) PBI and (b) PBI–CH_3OH complex. (c) The simulated Franck-Condon simulated spectrum of the PBI–CH_3OH complex is shown. The vertical dashed arrows in Trace b represent the progression of ν_{45} vibrational modes in combination with several other modes.

shown a large redshift.[19] Therefore, the 1211 cm^{-1} redshift of the 0_0^0 band in PBI-CH_3OH confirms the docking of the methanol molecule, similar to the water in the PBI-H_2O complex. The significant red shift also indicates the higher stability of the complex in the S_1 electronic state compared to that in the ground state.

In the case of PBI–CH_3OH, the ν'_{45} mode positioned at 99 cm^{-1} have shown a progression up to n=4. The band is the intramolecular in-plane bending motion of the PBI rings with respect to the C-C linkage (Figure 2). As reported earlier, the band is highly sensitive to the binding of the solvent to the PBI molecule. In the case of bare PBI and PBI-Ar complex (Figure 1a), the ν'_{45} modes were observed at the same position at 92 cm^{-1}. However, the band has shown a blue shift (95 cm^{-1}) in PBI-H_2O. The C-C linkage remained unaltered in the PBI-Ar complex. However, in PBI–H_2O complex with strongly bound $OH\cdots N_P$ and $N_IH\cdots O$ hydrogen bonds, the above ν'_{45} appeared in the higher energy region. The observed ν'_{45} at 99 cm^{-1} in PBI-CH_3OH supports the similar intermolecular structure of the complex to that of the PBI-H_2O.

Figure 2 shows the optimized geometry of the PBI-CH_3OH complex in the S_1 excited state with three other important vibrational modes. The calculations were done at the B3LYP/def2-TZVPP level of theory. The most stable PBI-CH_3OH structure shows hydrogen-bonded linkages between PBI and the solvent molecules as $OH\cdots N_P$ and $N_IH\cdots O$, with a bond distance of 1.62 Å and 1.65 Å, respectively. The above structure supports the experimental expectation discussed above. A similar structure was also reported earlier based on IR-UV double resonance spectroscopic investigations.[25]

The calculated structures (in both S_0 and S_1 states) were used to simulate the Franck-Condon activity of the $S_0 \rightarrow S_1$ transitions using the FC-LabWin program. The simulated spectrum with the calculated and scaled frequencies (0.763) shows a good agreement with the position of the experimentally measured spectrum (Figure 1c, Table 1). Note that the scaling is important to account for the anharmonicity

Table 1. The experimental band positions and the vibrational frequencies in excited (ν'_{Expt}) states of the PBI-CH_3OH and PBI-CH_3OD complexes are listed $cm^{-1,}$ along with the possible assignments. The intensity ratios of I_D/I_H, i.e., PBI-CH_3OD to PBI-CH_3OH complexes, are given. Frequency values in bold represent intramolecular vibrational modes.

PBI-CH_3OH		PBI-CH_3OD		Assignment	
Origin	30400	30413		0_0^0	
$\Delta\nu$ (cm^{-1})	−1211	−1198			
Positions	**Freq**	**Positions**	**Freq**	**Assignment**	**I_D/I_H**
30475	75	30490	**77**	$R_{CH_3}{}_0^1$	1.83
30479	79	30494	81	$R'_{CH_3}{}_0^1$	1.42
30485	85	30498	85	-	1.22
30497	**97**	30512	**99**	45_0^1	1.05
30549	149	30564	151	-	1.32
30564	164	30578	165	T_{x0}^1	2.05
30571	171	30583	170	$R_{CH_3}{}_0^1 45_0^1$	1.29
30585	185	30597	184	T_{y0}^1	1.65
30599	**199**	30610	**197**	45_0^2	1.64
30647	247	30662	249	-	1.92
30657	257	30669	256	-	2.00
30664	264	30676	263	-	3.55
30670	270	30682	269	-	2.17
30677	**277**	30689	**276**	45_0^3 (?)	3.04
30721	321	30733	320	T_{x0}^2	2.22
30732	332	30746	333	-	2.69
30745	345	30760	347	-	3.50
30762	362	30776	363	$T_{x0}^1 45_0^2$	2.50
30776	376	30789	376	-	2.70
30790	**390**	30802	**389**	45_0^4	2.27
		30840	**427**	-	-
		30853	**440**	-	-
		30886	**473**	-	-
		30900	**487**	45_0^5	-
		30947	**534**	-	-
		30965	**552**	-	-
		31003	**590**	45_0^6	
		31016	**603**	-	-
		31023	**610**	-	-
		31064	**651**	-	-
		31095	**682**	45_0^7	-
		31114	**701**	-	-
		31159	**746**	-	-
		31279	**866**	-	-

of the lower energy modes and the computational limitations. Here the scaling factor was obtained from the ratio of the experimental and calculated ν'_{45} mode. The simulated spectrum in Figure 1c has shown a good agreement with the band positions only. As shown in the figure 1c, The calculated intensity of the transitions to higher vibrational bands are significantly stronger than the experimental bands. Similar observations were previously reported for the PBI-H_2O complex.[19] Based on the comparison, the R2PI spectrum of the PBI-CH_3OH complex in Figure 1 shows $\nu'(R_{CH3})$ and ν'_{Tx} modes at 75 cm^{-1} and 164 cm^{-1}, respectively. The above modes are the internal rotation of the CH_3 group of methanol $\nu'(R_{CH3})$ and the internal translational motion of the solvent molecule along the $N_IH\cdots O$ coordinate ν'_{Tx} (as shown in Figure 2), respectively. The calculated ν'_{Tx} value (168 cm^{-1}) is in good agreement with the experimentally measured frequency (164 cm^{-1}). The ν'_{Ty} is the internal translational motion along the $OH\cdots N_P$ vibrational mode at 185 cm^{-1} is close to the calculated band at 182 cm^{-1}(see SI Table S1)). Like the PBI-H_2O complex, the higher value of ν'_{Ty} than the ν'_{Tx} suggests a stronger $OH\cdots N_p$ hydrogen bond than that of $N_IH\cdots O$ in the PBI-CH_3OH complex. The above is in line with the shorter $N_IH\cdots O$ hydrogen bond length.

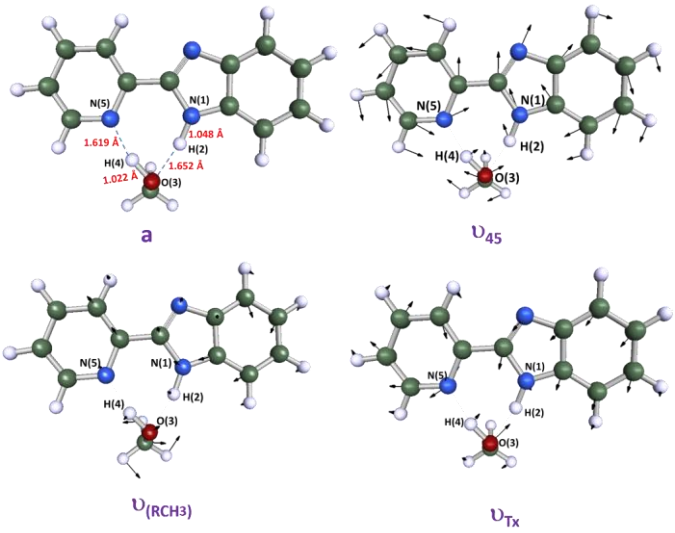

Figure 2. The structure 'a' is the geometry-optimized structure of PBI-CH_3OH in the S_1 state. The low energy vibrational modes in the PBI-CH_3OH complex in the S_1 state: (i) ν_{45} is the symmetric in-plane bending with respect to the C-C linkage between the pyridyl and imidazolyl groups; (ii) $\nu_R(CH_3)$ is the internal rotation of the CH_3 group of methanol in the complex; (iii) ν_{Tx} is the internal translation of the CH_3OH in the complex along N(1)-H(2)···O(3) (or $N_IH\cdots O$) hydrogen bond.

As mentioned earlier, the intensities of the transitions within 150 to 400 cm^{-1} above the origin band in the R2PI spectrum of PBI-CH_3OH is significantly reduced compared to the Franck-Condon simulated intensity, as shown in Figure 1c. The last observed band in Figure 1b is positioned at 0_0^0+390 cm^{-1}, which is also assigned as the 45_0^4. No other bands were detected above the region, even though the simulated Franck-Condon spectrum provide non-zero factors for many other higher energy vibrational modes.

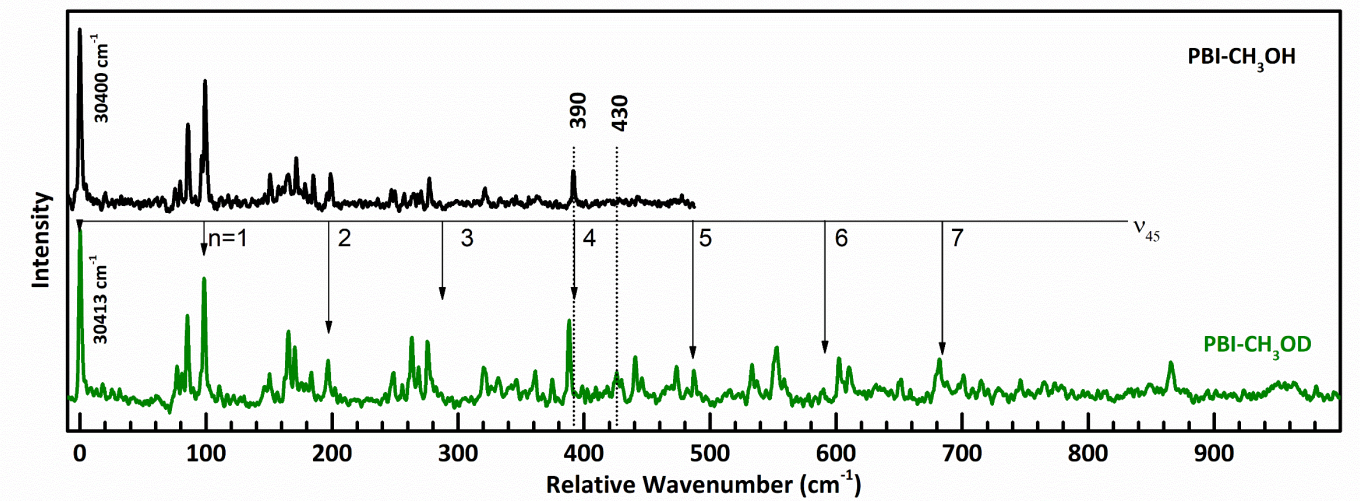

Figure 3. Two-colour resonant two-photon ionization spectra of the $S_0 \rightarrow S_1$ transitions of the PBI–CH_3OD complex is compared against that of the PBI-CH3OH complex. The vertical arrows represent the progression of ν_{45} modes till n=6.

In order to verify the reason for such band disappearance, we have measured the R2PI spectrum of the PBI-CH_3OD complex, as shown in Figure 3. The positions of the bands are given in Table 1, along with the assignments. The band origin of the complex is positioned at 30413 cm^{-1}, with the $\Delta\nu$ values at 1198 cm^{-1}. Both the values are nearly similar to that of the PBI-CH_3OH complex. Similarly, the vibrational modes in the S_1 state are found to be within ± 2 cm^{-1} of the bands detected in the PBI-CH_3OH system. The above implies a negligible effect of the isotopic substitution on the electronic structure of the complex in the ground and excited states. The vibrational modes 150-390 cm^{-1} region have shown relatively more intense R2PI bands in the PBI-CH_3OD complex than that in the PBI-CH_3OH system, as shown in Figure 3. The above can be explained only if the molecules in ν' levels of PBI-CH_3OH complex exhibit significantly lower lifetimes than the pulsed width of the laser (5-6 ns). The shorter lifetime of the above-mentioned vibrational states can be due to the enhanced quantum mechanical tunneling due to the proton/hydrogen atom transfer reaction.[1,12,28]

Note that, the increased intensity of the same bands in PBI-CH_3OD spectra clearly indicates the higher vibrational state lifetimes in the S_1 states upon isotopic substitution. Because the isotopic substitution has a greater mass, the zero-point vibrational energy of the complex can be reduced; as a result, the activation energy can be increased. Previous studies of the 7-hydroxyquinoline-$(CH_3OH)_2$ system demonstrated 8-16 kJ mol^{-1} increase in the activation energy of NH···O and OH···O double proton transfer barrier.[29] Both the above factors, the increase in the energy barrier and tunnelling mass, strongly suggest that the rate of D/D^+ tunneling in the PBI-CH_3OD complex can be drastically reduced compared to that of H/H^+ in the PBI-CH_3OH complex.[30] Therefore, the reduced tunneling effect can increase the lifetime of the ν' levels, which is evident from the R2PI spectrum of PBI-CH_3OD. To verify the extent of tunneling in CH_3OH, compared to CH_3OD, we have compared the intensity patterns of the bands within 0-500 cm^{-1} in the R2PI spectra of the respective PBI complex, as shown in Figure S1. The intensity ratios I_D/I_H the respective peaks are calculated from the normalized R2PI spectral band intensities of PBI-CH_3OD with that of PBI-CH_3OH as:

$$\frac{I_D}{I_H} = \frac{I_{PBI-CH_3OD}}{I_{PBI-CH_3OH}}$$

The obtained ratios are given in Table 1. The intramolecular bands at 99 and 197 cm^{-1} have shown I_D/I_H ratios of 1.05 and 1.64, respectively. The intermolecular bands in the same region, positioned at 165 (ν_{Tx}) and 249 ($\nu(R_{CH3})+\nu_{Tx}$), have relatively higher ratios (~2.0). Therefore, in the PBI-CH_3OH complex, the intermolecular modes undergo enhanced quantum tunnelling. Similarly, as shown in SI Figure S1 and Table 1, the higher energy bands, positioned > 300 cm^{-1}, have shown ID/IH values ranging >2.5 for most of the intermolecular bands, except the intramolecular band at 390 cm^{-1}. Based on the above data, we can confirm that the quantum mechanical tunnelling in the PBI-CH_3OH system is highly induced by intermolecular vibrational motion. The intramolecular band at 390 cm^{-1} has shown a high I_D/I_H ratio of 2.27 (SI Figure S1). In addition to the above, the absence of any intramolecular modes above $0_0^0 + 390$ cm^{-1} region must be due to the proximity of an excited state energy barrier rather than the effect of only the quantum tunnelling.

The R2PI spectrum of the PBI-CH_3OD Complex in Figure 3 shows vibrational bands up to $0_0^0 + 981$ cm^{-1}, and a progression of the ν_{45} mode is detectable till n=7. The above confirms the Franck-Condon activity of $S_0 \rightarrow S_1$ transition in the methanol complex at least until 981 cm^{-1} above the origin band. Therefore, the disappearance of the R2PI bands above 390 cm^{-1} in the PBI-CH_3OH complex cannot be termed as a loss of Franck-Condon activity. Note that the binding energy of the complex in the excited state is 55 kJ $mole^{-1}$ (4600 cm^{-1}, Table 2); therefore, the complexes cannot be dissociated at such

a low energy excitation. The most likely reason is the significant lowering of the excited vibrational state's lifetime in CH_3OH-complex as the excitation energy is higher than the associated energy barrier to either the proton or hydrogen atom transfer in the excited state. Therefore, the last band observed in the PBI-CH_3OH complex at 390 cm^{-1} is considered the lower limit of the energy barrier. The adjacent higher energy intramolecular band at 430 cm^{-1} in PBI-CH_3OD is considered the upper limit of the excited state energy barrier. Combining the above, the binding energy is experimentally measured as 410±20 cm^{-1}.

Table 2. Energies of the initial, transition state, final structures of PBI-CH_3OH complex along the hydrogen/proton transfer pathway calculated at DFT-D4 (B3-LYP/def2-TZVPP) level of theory.

Structure	Binding Energy	Relative energy (kJ $mole^{-1}$)	
	$D_e(S_1)$ ($D_0(S_1)$)	$\Delta E_R(S_0)$	$\Delta E_R(S_1)$
a (S_0)	52 (45)	0	0
a (S_1)	70 (55)	0	0
TS_{HT}	-	+ 88	+ 10
b	297 (285)	+ 79	- 86
TS_{PT}	-	0	+ 6
d	173 (171)	+ 200	- 103
e	223 (217)	+ 153	- 153

Excited state potential energy surfaces: The potential energy surface (PES) calculation along the concerted hydrogen atom transfer pathway N(1)-H(2)···O(3) (i.e., $N_IH\cdots O$) and O(3)-H(4)···N(5) (i.e., $OH\cdots N_p$) in both S_0 and S_1 states of PBI-CH_3OH complex are shown in Figure 4. The geometry-optimized structure of the tautomer form (structure 'b') in the S_1 state of the PBI-CH_3OH complex and the highest energy structure, namely 'TS' is also shown in the figure. As shown in Figure 4, the tautomer structure 'b' is 86 kJ $mole^{-1}$ (Table 2) more stable in the S_1 state than the normal form 'a'. As shown in Table 2, the excited state energy barrier is only 10 kJ mol^{-1}.

In order to verify the nature of the calculated reaction along the reaction path, we have calculated the excited state NBO charge on the CH_3O species of each structure along the path shown in Figure 4. A hydrogen atom transfer is expected to keep the NBO charge on CH_3O species unaltered along the path. However, a proton transfer pathway must be associated with the gain of electron density (-ve charge) on CH_3O. The relative NBO charge on CH_3O with respect to the starting structure-a is plotted in Figure 4 (empty blue circles). The charges on CH_3O along the reaction coordinate show a marginal loss of electron (+ve charge) on the species. The above confirms that the excited state reaction proceeds via the excited state hydrogen atom transfer. The small positive charge on the transition is most likely due to the strong electrostatic nature of the hydrogen bonding interactions in the transition state, in which the electronic charge on O-atom is shared with two close-range hydrogen atoms.

In order to verify the effect of triplet state on the reaction, we have calculated the energy of the T_1 state at the geometry of the S_1 state, and the same is shown in Figure 4. Along the reaction pathway, the triplet state remained much lower in energy compared to the singlet states till the transition state. The intersystem crossing is only feasible at a structure beyond the transition state along the hydrogen atom transfer and hence should not actively intervene in the reaction progress. Therefore, the excited state hydrogen atom transfer reaction requires an energy of 10 kJ mol^{-1} in the S_1 state. The experimentally determined energy barrier of 410±20 cm^{-1} (4.91±0.23 kJ mol^{-1}) is nearly half of that of the calculated value. Note that the tautomer structure (b in Figure 4) is 79 kJ mol^{-1} less stable than the normal form 'a' in the ground state, and the tautomerization reaction is not feasible in the ground state as the energy barrier is calculated as + 88 kJ mol^{-1}.

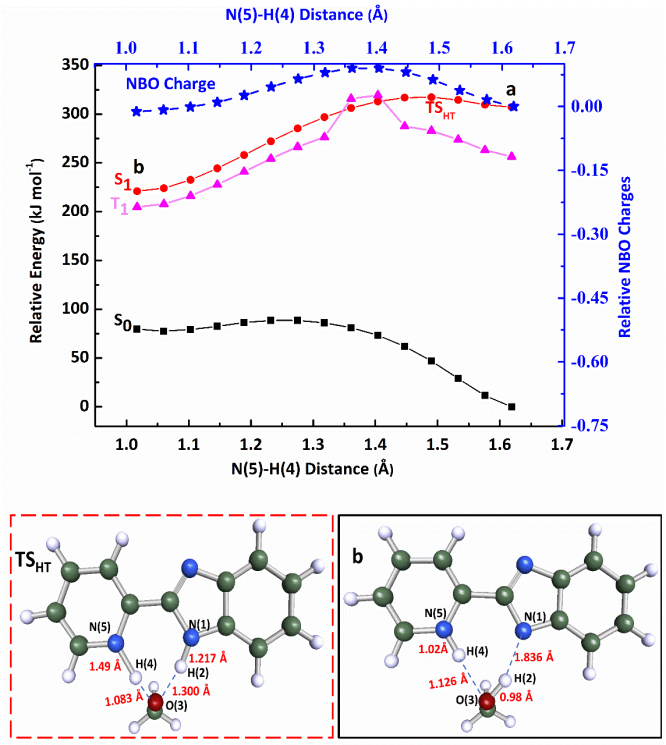

Figure 4. DFT-D4 (B3-LYP/def2-TZVPP) computed potential energy surface along the hydrogen transfer pathway in both the electronic ground (S_0), the excited (S_1) states and (T_1) states of the PBI–CH_3OH as a function of the concerted stretching of the N(5)-H(4)and N(1)-H(2) distances. The structures of the TS_{HT} and tautomer b with important bond distances are also given. The relative NBO charge on CH_3O moiety with respect to the structure-a along the pathway are shown (values are on the right Y-axis).

The proton transfer reaction product was generated by optimizing the hydrogen-bonded structure of $PBIH^+$ and CH_3O^- in the ground state. The geometry-optimized structure is shown as PT in Figure 5. The PES of the proton transfer reaction in the ground state, from the PBI-CH_3OH complex to PT, is shown in Figure 5. The above reaction path is found to be a barrierless climbing in energy. Therefore, the forward reaction, i.e., deprotonation of CH_3OH by PBI, is not feasible in

the ground state. The vertical excitation energy of the structures along the pathway, as shown in Figure 5, provides information on the variation of various excited electronic states along the pathway. Detailed analysis of the molecular orbital diagrams of each structure helped us to assign the nature of the electronically excited states. The energy of the lowest excited singlet ππ* state of the PBI-CH_3OH complex increases along the reaction coordinate. Interestingly, the energy of the excited nπ* state gradually decreases along the path and becomes the lowest singlet energy excited state of the PT structure. The point at which the ππ* and nπ* intersects are found with the structure-c (Figure 5) with shorter $N_P\cdots H$ bond lengths of 1.274 Å compared to that of 1.619 Å in the PBI-CH_3OH structure. Additionally, the nπ* state is highly stable than the excited PBI-CH_3OH (ππ* state). The above information implies possible deprotonation of the methanol by an excited state PBI molecule.

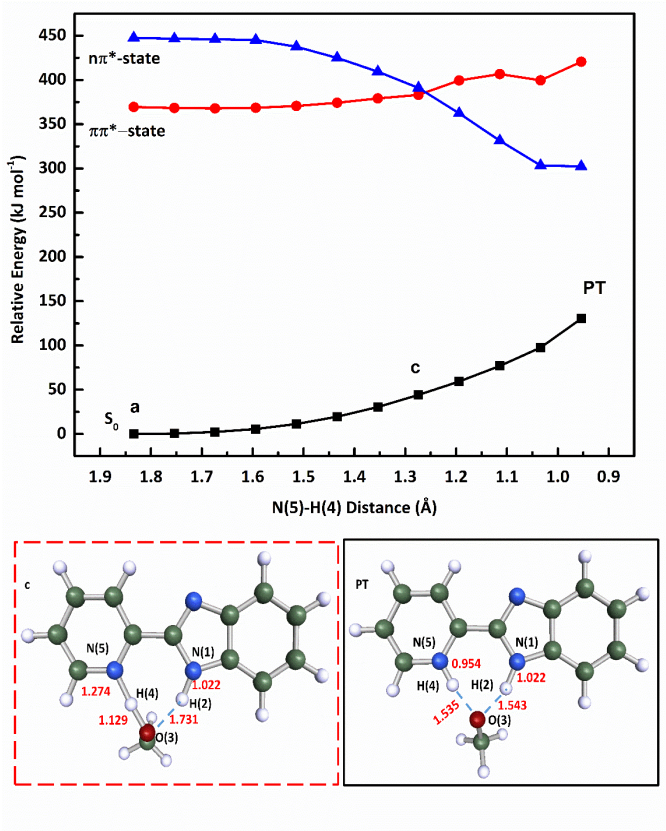

Figure 5. DFT-D4 (B3-LYP/def2-TZVPP) computed potential energy surface for the electronic ground state (S_0) and the locally excited (S_1) state of the PBI–CH_3OH as a function of the concerted stretching of the N(5)-H(4) distances. The optimized structures of the proton transfer product (PT) and the structure at which the ππ* and nπ* intersects (c) are given.

To calculate the energy barrier in the excited state along the proton transfer reaction pathway, a PES scan was executed along the $OH\cdots N_p$ by constraining the $N_iH\cdots O$ bond distance at 1.022 Å (identical to that in structure e), as shown in Figure 6. The structures of marked points in the PES are given in Figure 7. The structures d and e represent different forms of the proton transfer products (PT structures) in the excited states. The above structures, as shown in Table 2, are found to be 103 and 153 kJ mol^{-1} more stable than the PBI-CH_3OH in the S_1 state. Additionally, the energies of the structures d and e in the ground and excited states are nearly identical, which indicates an efficient internal conversion of the excited state along the proton transfer coordinates. The calculated ESPT energy barrier is 6 kJ mol^{-1} in the S_1 state. The above energy barrier is less than that calculated for the ESHT reaction pathway (10kJ $mole^{-1}$). Additionally, the experimental energy barrier of 410±20 cm^{-1} (4.91±0.23 kJ mol^{-1}) in the PBI-CH_3OH system is found to be in excellent agreement with the calculated barrier (6 kJ mol^{-1}).

To confirm the proton transfer reaction along the pathway in the excited state, charge properties were calculated using NBO analysis. The relative NBO charge on CH_3O species (with respect to structure a), as shown in Figure 6, is gradually becoming more negative along the coordinate. The above negative charge accumulation on the CH_3O species confirms the proton transfer to the PBI molecule by leaving the electron on the solvent species. The negative charge rapidly increases beyond the transition state till the proton transfer structures d and/or e (Figure 7).

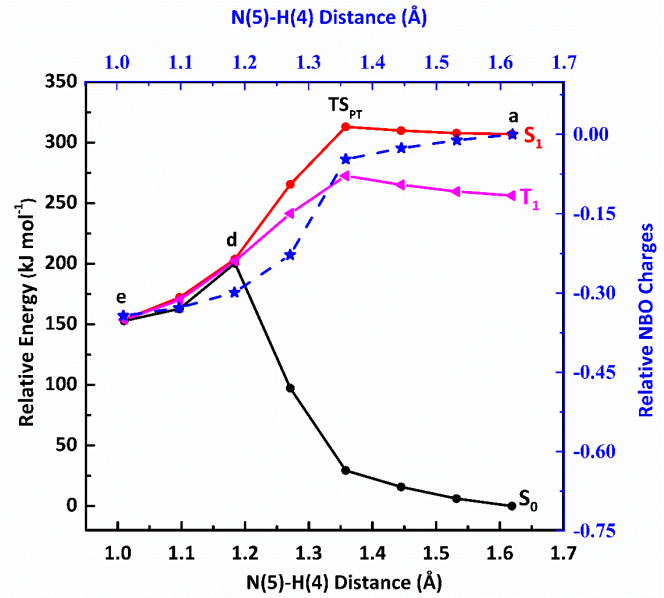

Figure 6: DFT-D4 (B3-LYP/def2-TZVPP) computed potential energy functions for the electronic ground (S_0) state (black lines), the electronically excited (S_1) state (red lines) as a function of the N (5)–H (4) distance along the proton-transfer coordinate are given. The corresponding energy at the T_1 state (triplet) (red dotted lines) of PBI–CH_3OH for the reaction path optimization (red lines). The relative NBO charge on CH_3O moiety with respect to the structure-a along the pathway are shown (values are on the right Y-axis).

To understand the properties of the electronic states, molecular orbitals of the structures are shown in Figure 7. The excited states

of both the structure 'a' and TS_{PT} are found to be ππ* states, whereas, for both d and e, the state is an nπ* state, with the n-orbital located on the solvent-O atom. Therefore, the excited state proton transfer in the PBI-CH_3OH system occurs via the crossing of ππ* and nπ* states. Subsequently, the system undergoes rapid internal conversion for deactivation. The above internal conversion processes can decrease the lifetime of the excited state vibrational states drastically above the energy barrier. Additionally, to understand the contribution of the triplet state in the above reaction, the energy of the T_1 state at the S_1 geometries were calculated and are shown in Figure 6. Similar to the ESHT reaction pathway, the intersystem crossing is feasible only after crossing the energy barriers.

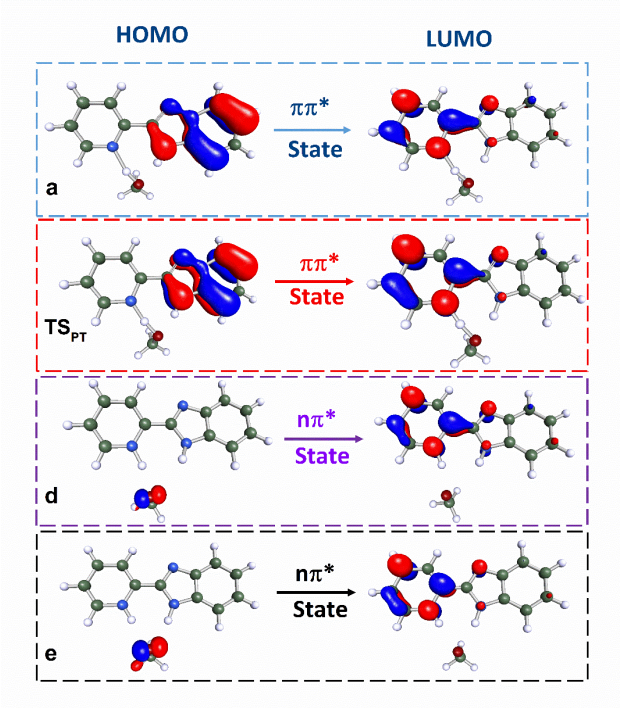

Figure 7: The HOMO–LUMO and the optimized structures of the initial, transition state and and PT products (d and e) are shown.

In both proton and hydrogen transfer potential energy scans, the highest energy obtained structure is considered as the transition state structure, and the energies are found to be 6 and 10 kJ $mole^{-1,}$ respectively. The ESPT energy barrier excellently agrees with the experimental value of 4.91±0.23 kJ mol^{-1}. The rapid decay of the excited state lifetime above the dissociation limit can be due to the internal conversion processes for the deactivation of the complex.

Detailed comparison of the experimental and computational results of the current system with that obtained from the PBI-H_2O and PBI-NH_3 complexes resulted in several key characteristics of the excited state processes. In the case of the PBI-NH_3 complex, no significant tunnelling was observed till 868 cm^{-1} (10.4 kJ mol^{-1}) because of increased potential width and higher energy barrier, where the ammonia molecule forms weak hydrogen bonding towards the Pyridyl-N group. In the above system, the calculation also predicted a marginal preference for excited state hydrogen transfer reaction compared to the proton transfer process. The ESPT energy barriers in PBI-H_2O complex was measured at 431 ± 10 cm^{-1} (5.2±0.1 $kJmol^{-1}$). Compared to the PBI-H_2O complex, the PBI-CH_3OH complex showed enhanced tunnelling due to the stronger association of the hydrogen bonded complex with a short distance. The energy barrier of 4.91±0.23 kJ mol^{-1} in the PBI-CH_3OH complex is also lower than that of the water complex. Therefore, a better hydrogen bond donor solvent, such as water and methanol, displays an efficient solvent-to-chromophore excited state proton transfer pathway, which leads to the deactivation of the photo-excited state. Detail description of the novel deactivation mechanism required a large set of experimental data, which is lacking in the literature.

Conclusions

The current article demonstrates evidence of solvent-to-chromophore excited state proton transfer process. Experimental proof of such novel reaction pathway is limited in the literature. Here, we have investigated the excited state processes in PBI-CH_3OH and PBI-CH_3OD complexes using resonant two-colour two-photon ionization spectroscopy, and computational investigations. The PBI contains both the basic N and acidic N-H groups that can be bridged via hydrogen bonding with a methanol molecule to facilitate the proton transfer reaction upon UV photoexcitation. The significant red shifted band origin and the experimental lower energy vibrational modes agree excellently with the values calculated using the above geometry of the complex.

The underlying reaction pathway was probed by measuring the energy barriers in the excited state processes. The measured ESPT energy barrier of 4.91±0.23 kJ mol^{-1} is nearly similar to that calculated using B3LYP-D4/def2-TZVPP level of theory (6.0 $kJmol^{-1}$). To confirm the solvent proton transfer process, isotopically labeled solvent molecule were used and the R2PI spectrum of PBI-CH_3OD complex were recorded. The above system has shown a reduced tunneling effect on the spectrum due to the increase in the tunneling mass and significantly enhanced energy barrier (due to the ZPVE stabilization). The kinetic isotope effect on the each spectral band in the PBI-CH_3OD complex reveals that the tunnelling of a proton is enhanced on the intermolecular modes compared to that in intramolecular modes.

Further, we have investigated the fate of the excited state process computationally, aided by experimental observations. The short lifetime of the inter and intramolecular modes above the energy barrier is due to internal conversion. The reaction proceeds via the intersection of ππ* and nπ* state before the internal conversion similar to the PBI-H_2O complex. The comparison of the above processes in PBI-CH_3OH with that in the PBI-H_2O and PBI-NH_3 complexes suggests that the solvent with higher gas-phase acidity can easily undergo deactivation via solvent-to-chromophore excited state proton transfer mechanism. Overall, the reaction mechanism can be considered as the key process using which a UV-excited biomolecule can protect itself via fast deactivation to the

ground state. The above theory requires detailed investigations of such processes using ultrafast lasers and high computational calculations.

Author Contributions

JR, SK, and MS performed the experiments while JR and SK did the analysis and computational work. JR has written the draft with the help of SM.

Conflicts of interest

There are no conflicts to declare.

Acknowledgements

This work has been supported by the Department of Chemistry, IIT Hyderabad, and MHRD, the Government of India. SK and MS thank MHRD, India, for the research fellowship. JR thanks UGC for the research fellowship. SM expresses sincere gratitude towards Prof. Samuel Leutwyler, the University of Bern, for his generous instrumentation aid to IITH for the experimental setup. SM thanks SERB, DST government of India (Grant no. CRG/2019/003335) for funding.

References

1 T. Schultz, E. Samoylova, W. Radloff, I. V. Hertel, A. L. Sobolewski and W. Domcke, Efficient deactivation of a model base pair via excited-state hydrogen transfer, *Science (80-.).*, 2004, **306**, 1765–1768.

2 W.-M. M. Kwok, C. Ma and D. L. Phillips, Femtosecond Time- and Wavelength-Resolved Fluorescence and Absorption Spectroscopic Study of the Excited States of Adenosine and an Adenine Oligomer, *J. Am. Chem. Soc.*, 2006, **128**, 11894–11905.

3 J. M. L. Pecourt, J. Peon and B. Kohler, DNA excited-state dynamics: Ultrafast internal conversion and vibrational cooling in a series of nucleosides, *J. Am. Chem. Soc.*, 2001, **123**, 10370–10378.

4 C. E. Crespo-Hernández, B. Cohen, P. M. Hare and B. Kohler, Ultrafast Excited-State Dynamics in Nucleic Acids, *Chem. Rev.*, 2004, **104**, 1977–2020.

5 W. J. Schreier, P. Gilch and W. Zinth, Early Events of DNA Photodamage, *Annu. Rev. Phys. Chem.*, 2015, **66**, 497–519.

6 Y. Zhang, K. de La Harpe, A. A. Beckstead, L. Martínez-Fernández, R. Improta and B. Kohler, Excited-State Dynamics of DNA Duplexes with Different H-Bonding Motifs, *J. Phys. Chem. Lett.*, 2016, **7**, 950–954.

7 X. Wang, Y. Yu, Z. Zhou, Y. Liu, Y. Yang, J. Xu and J. Chen, Ultrafast Intersystem Crossing in Epigenetic DNA Nucleoside 2′-Deoxy-5-formylcytidine, *J. Phys. Chem. B*, 2019, **123**, 5782–5790.

8 X. Wang, Z. Zhou, Y. Tang, J. Chen, D. Zhong and J. Xu, Excited State Decay Pathways of 2′-Deoxy-5-methylcytidine and Deoxycytidine Revisited in Solution: A Comprehensive Kinetic Study by Femtosecond Transient Absorption, *J. Phys. Chem. B*, 2018, **122**, 7027–7037.

9 R. Knochenmuss and I. Fischer, Excited-state proton transfer in naphthol/solvent clusters: The current state of affairs, *Int. J. Mass Spectrom.*, 2002, **220**, 343–357.

10 R. Knochenmuss, O. Cheshnovsky and S. Leutwyler, Proton transfer reactions in neutral gas-phase clusters: 1-Naphthol with H2O, D2O, CH3OH, NH3 and piperidine, *Chem. Phys. Lett.*, 1988, **144**, 317–323.

11 C. Tanner, C. Manca and S. Leutwyler, Probing the Threshold to H Atom Transfer Along a Hydrogen-Bonded Ammonia Wire, *Science (80-.).*, 2003, **302**, 1736–1739.

12 E. Samoylova, V. R. Smith, H. H. Ritze, W. Radloff, M. Kabelac and T. Schultz, Ultrafast deactivation processes in aminopyridine clusters: Excitation energy dependence and isotope effects, *J. Am. Chem. Soc.*, 2006, **128**, 15652–15656.

13 A. Douhal, S. K. Kim and A. H. Zewail, Femtosecond molecular dynamics of tautomerization in model base pairs, *Nature*, 1995, **378**, 260–263.

14 C. Jouvet, M. Miyazaki, M. Fujii, M. Mitsuhiko and M. Fujii, Revealing the role of excited state proton transfer (ESPT) in excited state hydrogen transfer (ESHT): systematic study in phenol–(NH 3) n clusters, *Chem. Sci.*, 2021, **12**, 3836–3856.

15 K. Sakota, C. Okabe, N. Nishi and H. Sekiya, Excited-state double-proton transfer in the 7-azaindole dimer in the gas phase. 3. Reaction mechanism studied by picosecond time-resolved REMPI spectroscopy, *J. Phys. Chem. A*, 2005, **109**, 5245–5247.

16 K. Sakota and H. Sekiya, Excited-state double-proton transfer in the 7-azaindole dimer in the gas phase. 2. Cooperative nature of double-proton transfer revealed by H/D kinetic isotopic effects., *J. Phys. Chem. A*, 2005, **109**, 2722–2727.

17 X. F. Yu, S. Yamazaki and T. Taketsugu, Solvent effects on the excited-state double proton transfer mechanism in the 7-azaindole dimer: A TDDFT study with the polarizable continuum model, *Phys. Chem. Chem. Phys.*, 2017, **19**, 23289–23301.

18 S. Takeuchi and T. Tahara, Femtosecond ultraviolet-visible fluorescence study of the excited-state proton-transfer reaction of 7-azaindole dimer, *J. Phys. Chem. A*, 1998, **102**, 7740–7753.

19 S. Khodia and S. Maity, A combined experimental and computational study on the deactivation of a photo-excited 2,2′-pyridylbenzimidazole–water complex via excited-state proton transfer, *Phys. Chem. Chem. Phys.*, 2022, **24**, 12043–12051.

20 S. Khodia, J. Ramesh and et al., Excited State Deactivation via Solvent to Chromophore Proton Transfer in Isolated 1:1 Molecular Complex: Experimental Validation By Measuring the Energy Barrier and Kinetic Isotope Effect, *PCCP*, , DOI:10.1039/D3CP00805C.

21 P. R. Chowdhury, S. Khodia and S. Maity, Solvent assisted excited-state deactivation pathways in isolated 2, 7-diazaindole-S1-3 (S= Water and Ammonia) complexes, *Spectrochim. Acta Part A Mol. Biomol. Spectrosc.*, 2022, **278**, 121285.

22 P. J. Linstrom and W. G. Mallard, The NIST Chemistry WebBook: A chemical data resource on the internet, *J. Chem. Eng. Data*, 2001, **46**, 1059–1063.

23 S. G. Balasubramani, G. P. Chen, S. Coriani, M. Diedenhofen, M. S. Frank, Y. J. Franzke, F. Furche, R.

Grotjahn, M. E. Harding, C. Hättig, A. Hellweg, B. Helmich-Paris, C. Holzer, U. Huniar, M. Kaupp, A. Marefat Khah, S. Karbalaei Khani, T. Müller, F. Mack, B. D. Nguyen, S. M. Parker, E. Perlt, D. Rappoport, K. Reiter, S. Roy, M. Rückert, G. Schmitz, M. Sierka, E. Tapavicza, D. P. Tew, C. Van Wüllen, V. K. Voora, F. Weigend, A. Wodyński and J. M. Yu, TURBOMOLE: Modular program suite for ab initio quantum-chemical and condensed-matter simulations, *J. Chem. Phys.*, 2020, **152**, 184107.

24 I. Pugliesi and K. Müller-Dethlefs, The use of multidimensional Franck-Condon simulations to assess model chemistries: A case study on phenol, *J. Phys. Chem. A*, 2006, **110**, 4657–4667.

25 M. Guin, S. Maity and G. N. Patwari, Infrared-optical double resonance spectroscopic measurements on 2-(2′-Pyridyl)benzimidazole and its hydrogen bonded complexes with water and methanol, *J. Phys. Chem. A*, 2010, **114**, 8323–8330.

26 S. Khodia and S. Maity, A combined spectroscopic and computational investigation on dispersion-controlled docking of Ar atoms on 2-(2′-pyridyl)benzimidazole, *Phys. Chem. Chem. Phys.*, 2021, **23**, 17992–18000.

27 Saurabh Khodia, Ramesh Jarupula and Surajit Maity, Accurate measurement of sequential Ar desorption energies from the dispersion-dominated Ar 1–3 complexes of aromatic molecules, *Phys. Chem. Chem. Phys.*, 2023, **25**, 2510–2516.

28 M. A. Trachsel, S. Blaser, L. Siffert, T. Wiedmer and S. Leutwyler, Excited-state vibrations, lifetimes, and nonradiative dynamics of jet-cooled 1-ethylcytosine, *J. Chem. Phys.*, 2019, **151**, 124301.

29 Y. Mori, Reaction pathway and H/D kinetic isotope effects of the triple proton transfer in a 7-hydroxyquinoline-methanol complex in the ground state: A computational approach, *J. Phys. Org. Chem.*, 2018, **31**, 1–12.

30 J. Meisner and J. Kästner, Atom tunneling in chemistry, *Angew. Chemie Int. Ed.*, 2016, **55**, 5400–5413.